

Analytic solution to pseudo-Landau levels in strongly bent graphene nanoribbons

Tianyu Liu,^{1,2} Roderich Moessner,¹ and Hai-Zhou Lu^{2,3}

¹Max-Planck-Institut für Physik komplexer Systeme, 01187 Dresden, Germany

²Institute for Quantum Science and Engineering and Department of Physics,
Southern University of Science and Technology, Shenzhen 518055, China

³Shenzhen Key Laboratory of Quantum Science and Engineering, Shenzhen 518055, China
(Dated: September 20, 2021)

Nonuniform elastic strain is known to induce pseudo-Landau levels in Dirac materials. But these pseudo-Landau levels are hardly resolvable in an analytic fashion when the strain is strong, because of the emerging complicated space dependence in both the strain-modulated Fermi velocity and the strain-induced pseudomagnetic field. We analytically characterize the solution to the pseudo-Landau levels in experimentally accessible strongly bent graphene nanoribbons, by treating the effects of the nonuniform Fermi velocity and pseudomagnetic field on equal footing. The analytic solution is detectable through the angle-resolved photoemission spectroscopy (ARPES) and allows quantitative comparison between theories and various transport experiments, such as the Shubnikov-de Haas oscillation in the complete absence of magnetic fields and the negative strain-resistivity resulting from the valley anomaly. The analytic solution can be generalized to twisted two-dimensional materials and topological materials and will shed a new light on the related experimental explorations and straintronics applications.

Introduction.— Landau levels [1] act as the canonical response of the orbital motion of electrons to the applied magnetic field and are the reason behind so many macroscopic quantum phenomena, such as the quantum Hall effect [2], quantum oscillations [3], and quantum anomalies [4–11]. The formation of Landau levels in Dirac materials such as graphene or Weyl semimetals, intriguingly, does not necessarily rely on magnetic fields as long as an appropriate elastic strain is applied [12–26]. Such strain displaces the Dirac cones in a space-dependent fashion analogous to magnetic fields and can thus induce low-energy pseudo-Landau levels that support quantum oscillations [27, 28] as well as the chiral anomaly and the associated chiral magnetic effect [29, 30]. In the simplest and most flexible Dirac material – graphene, the experimentally implementable strain can be as large as 27% [31, 32], and may be of various patterns, such as bend [33–35], twist [31, 36], and other simple uniaxial ones [37, 38].

Unfortunately, the pseudo-Landau levels induced by the aforementioned strain patterns are *dispersive* and thus are not directly interpretable by the standard Dirac theory established for the ordinary dispersionless Landau levels. For weak strain, the pseudo-Landau level dispersions are often overlooked for simplicity until a recent study [38] analytically solves such dispersions in a uniaxially strained graphene nanoribbon with a nonuniform Fermi velocity but a uniform pseudomagnetic field. Nevertheless, understanding how pseudo-Landau levels disperse in the presence of strong strain is a much more complicated problem remaining largely unexplored. This is presumably because the pseudo-Landau levels are expected to occupy a large portion of the Brillouin zone with increased strain; and the standard procedure solving pseudo-Landau levels using linearized Hamiltonians

[15, 16, 20–22, 33, 34, 37, 38] at the Brillouin zone corners consequently fails.

In this Letter, we present an approach to give analytic solution to the pseudo-Landau levels in bent zigzag graphene nanoribbons under strong strain. Our ground is that the hidden chiral symmetry [39] effectively maps the graphene nanoribbon unit cell [Fig. 1(a)] into a Su-Schrieffer-Heeger model [40] at any momentum k_x . For strain-free graphene nanoribbons, the Su-Schrieffer-Heeger topological end modes for certain k_x 's constitute the well-known zero-energy edge states. For bent graphene nanoribbons, the bipartite hoppings in the Su-Schrieffer-Heeger model are spatially modulated; and one of the zero-energy topological end modes is pushed into the bulk [Fig. 1(b)] and becomes a domain wall mode separating the topological and trivial sectors of the unit cell. We elaborate that this zero-energy state centered at the

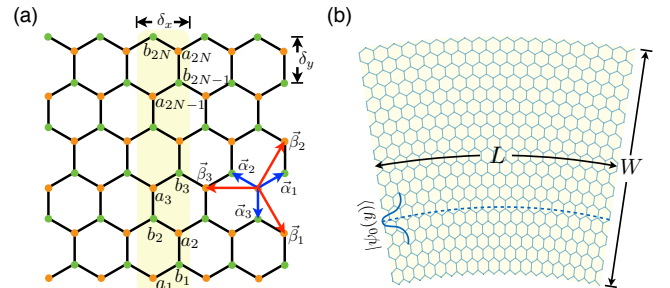


FIG. 1. (a) Schematic plot of an undeformed zigzag graphene nanoribbon. The yellow shadow marks the unit cell with bipartite hoppings in $a_j \leftrightarrow b_j$ and $b_j \leftrightarrow a_{j+1}$. (b) Schematic plot of a circularly bent graphene nanoribbon. The strain creates in the bulk a domain wall (dashed) at which the bipartite hoppings are identical. The localized domain wall state is the zeroth pseudo-Landau level $|\psi_0(y)\rangle$ by nature.

domain wall is the zeroth pseudo-Landau level by nature. In the vicinity of the domain wall (i.e., the common guiding center of the pseudo-Landau levels), we restore the eigenvalue problem into an analytically solvable standard Dirac equation through linearizing the model Hamiltonian. In contrast to the standard linearization around Brillouin zone corners, our linear expansion is conducted in *real* space. It thus treats the strain-modulated Fermi velocity and the strain-induced pseudomagnetic field on equal footing to give an accurate analytic solution to the pseudo-Landau levels in a wide range in the Brillouin zone. The analytic solution allows us to further explore the pseudo-Landau-level-mediated transport exemplified by the Shubnikov-de Haas oscillation in the absence of magnetic fields and the negative strain-resistivity resulting from the valley anomaly. Our techniques are transplantable to a variety of materials such as the twisted bilayer graphene and Dirac matter and may pave the way to straintronics applications.

Model.— We model a strain-free zigzag graphene nanoribbon [Fig. 1(a)] with the tight-binding Hamiltonian

$$H = \sum_{k_x, y} b^\dagger_{k_x, y + \frac{\delta_y}{6}} [2t_{1,2} \cos(\frac{1}{2}k_x \delta_x) + t_3 \hat{s}_{\delta_y}] a_{k_x, y - \frac{\delta_y}{6}} + \text{H.c.}, \quad (1)$$

where $\delta_x = \sqrt{3}a$ and $\delta_y = \frac{3}{2}a$ with $a = 1.42 \text{ \AA}$ being the lattice constant of the honeycomb lattice; \hat{s}_{δ_y} is a shift operator satisfying $\hat{s}_{\delta_y} a_{k_x, y} = a_{k_x, y + \delta_y}$; and $t_{1,2} = t$ ($t_3 = t$) is the hopping parameter along bond $\alpha_{1,2}$ (α_3) with $t = -2.8 \text{ eV}$ [41]. In the presence of bend [Fig. 1(b)], the hopping parameters are spatially modulated (Sec. SI of Ref. [42])

$$t_{1,2} \rightarrow t \exp \left\{ g \left[1 - \sqrt{\frac{3}{4}(1 + \lambda y)^2 + \frac{1}{4}} \right] \right\} \equiv t(y), \quad (2)$$

where λ is the curvature of nanoribbon and $g = 3.37$ is the Grüneisen parameter [43]. In the weak strain limit $\lambda y < \lambda W \ll 1$, a common practice [13–15, 21, 28, 33, 37, 38] is to estimate $t(y)$ to the linear order as $t(y) \approx t(1 - \frac{3}{4}g\lambda y)$. The subsequent linear expansion of Eq. (1) around the Brillouin zone corners $\mathbf{k}^\eta = (\eta \frac{4\pi}{3\sqrt{3}a}, 0)$ gives

$$h_{\mathbf{q}}^\eta = \hbar v_x^\eta (q_x - \eta \frac{g}{2a} \lambda y) \sigma^x + \hbar v_y^\eta q_y \sigma^y, \quad (3)$$

where $\eta = \pm 1$ is the valley index, $(v_x^\eta, v_y^\eta) = \frac{3ta}{2\hbar}(-\eta, 1)$ is the Fermi velocity, and $\mathbf{q} = \mathbf{k} - \mathbf{k}^\eta$ is measured from the Dirac points. The strain-induced pseudomagnetic field can be read off as $\mathcal{B}_z^\eta = \eta \frac{g\hbar}{2ea} \lambda$, leading to dispersionless pseudo-Landau levels $E_n^\eta = \pm \sqrt{2n|e\mathcal{B}_z^\eta \hbar v_x^\eta v_y^\eta|}$. However, such flat pseudo-Landau levels are insufficient to characterize the low-energy electronic structure consisted of slightly dispersive bands [Fig. 2(a)], because higher-order terms [e.g., $O(q_y q_x)$, $O(\lambda q_x)$, and $O(\lambda q_y q_x)$] in the expansion of Eq. (1) are also expected to affect the energy spectrum to the linear order of q_x . Supplemented by

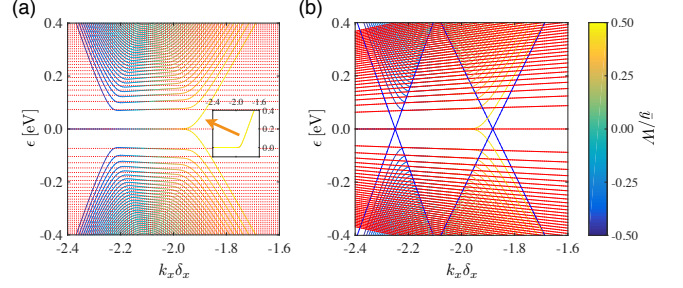


FIG. 2. Strain-induced pseudo-Landau levels in a bent graphene nanoribbon of width $W = 192 \text{ nm}$ and bend curvature $\lambda = 0.642 \mu\text{m}^{-1}$. (a) Numerically calculated bands (solid) in the vicinity of the K point $\mathbf{k} = (-\frac{2\pi}{3\delta_x}, 0)$ with theoretically proposed flat pseudo-Landau levels E_n^η (dotted) overlaid. The color code represents \bar{y} . The inset is to better illustrate the marked band whose flat sector is blocked due to degeneracy. (b) The same numerical bands overlaid by the slightly dispersive pseudo-Landau levels $\mathcal{E}_n^\eta(q_x)$ (red solid). The blue curves mark the maximally displaced Dirac cones.

these higher-order terms, $h_{\mathbf{q}}^\eta$ is modified to

$$h_{\mathbf{q}}^\eta = \hbar \tilde{v}_x^\eta (q_x - \eta \frac{g}{2a} \lambda y) \sigma^x + \hbar \tilde{v}_y^\eta q_y \sigma^y, \quad (4)$$

where the Fermi velocity becomes nonuniform with $\tilde{v}_x^\eta = v_x^\eta (1 - \frac{3}{4}g\lambda y)$ and $\tilde{v}_y^\eta = v_y^\eta (1 + \frac{1}{2}\eta q_x a - \frac{1}{4}g\lambda y - \frac{3}{8}\eta q_x a g \lambda y)$, but the pseudomagnetic field is intact to the lowest order of y . The spectrum of $h_{\mathbf{q}}^\eta$ comprises of slightly dispersive pseudo-Landau levels $\mathcal{E}_n^\eta(q_x) = E_n^\eta (1 + \frac{3}{2}\eta q_x a)^{1/2}$ [38], which indeed better capture the energy bands in Fig. 2(b). It is worth noting that $\mathcal{E}_n^\eta(q_x)$ only characterizes the bulk bands bounded between the two maximally displaced Dirac cones $\epsilon_{\text{max}}^{\text{DC}} = \pm \hbar \tilde{v}_x^\eta (q_x - \eta \frac{g}{2a} \lambda y)|_{y=\pm W/2}$, while dispersive marginal bands and flat edge bands appear in and outside the maximally displaced Dirac cones, respectively (Sec. SIII of Ref. [42]). The positions of the energy bands are reflected by the average of the position operator \bar{y} .

Band topology analysis.— We first determine the positions of pseudo-Landau levels in the real space by analyzing the band topology of a bent graphene nanoribbon with a *generic* strain strength. According to Eqs. (1) and (2), at a given momentum k_x , the unit cell of the nanoribbon is a Su-Schrieffer-Heeger model [40] with intracell hopping $2t(y) \cos(\frac{1}{2}k_x \delta_x)$ and intercell hopping t . For momenta $|k_x| \leq \frac{2}{\delta_x} \arccos(\frac{1}{2}e^{-g/2})$, a domain wall appears at

$$l_0 = \frac{1}{\lambda} \left\{ \sqrt{\frac{4}{3} \{ 1 + g^{-1} \ln[2 \cos(\frac{1}{2}k_x \delta_x)] \}^2 - \frac{1}{3} - 1} \right\}, \quad (5)$$

where the two hoppings are identical. The position of the domain wall has a profound influence on the band topology. For $\lambda = 0$, the domain wall can only be located within the nanoribbon at the Dirac points. For $|k_x| > \frac{2\pi}{3\delta_x}$ ($|k_x| < \frac{2\pi}{3\delta_x}$), the unit cell becomes a topological (trivial)

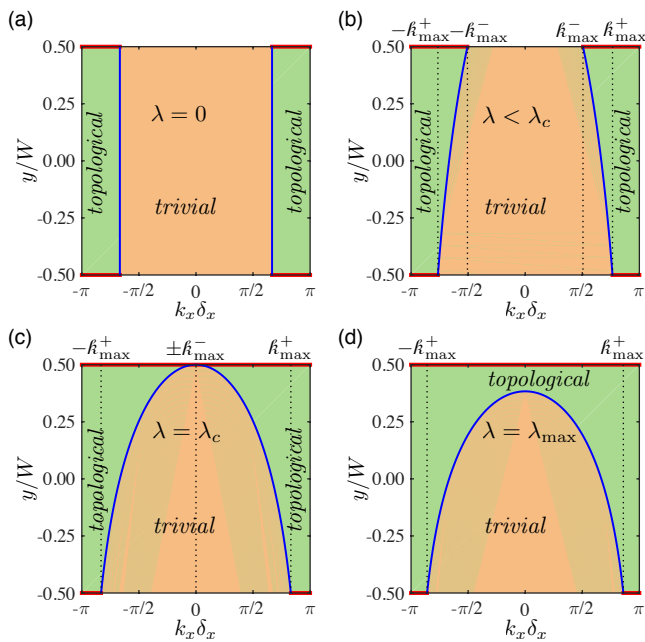


FIG. 3. Phase diagrams of a bent graphene nanoribbon of a generic width W . (a) An undeformed nanoribbon with $\lambda = 0$. (b) A moderately bent nanoribbon with $\lambda W = 0.263$. (c) A critically bent nanoribbon with $\lambda_c W = 0.534$. (d) A maximally bent nanoribbon with $\lambda_{\max} W = 0.696$. In each panel, the blue curve between the dashed lines marks the position of the Su-Schrieffer-Heeger domain wall [Eq. (5)]; and the green (orange) patch above (below) the blue curve labels the topological (trivial) segment of the nanoribbon unit cell. The topological segments also produce zero-energy edge states as indicated by the bold red lines at both the stretched edge ($y = W/2$) and the compressed edge ($y = -W/2$).

Su-Schrieffer-Heeger chain [Fig. 3(a)]. For $0 < \lambda < \lambda_c$, where $\lambda_c = \frac{2}{W} \{ [\frac{4}{3}(1+g^{-1} \ln 2)^2 - \frac{1}{3}]^{1/2} - 1 \} = 0.534W^{-1}$, the domain wall is located within the nanoribbon at the momenta satisfying $\hbar_{\max}^- \leq |k_x| \leq \hbar_{\max}^+$, where $\hbar_{\max}^\pm = \frac{2}{\delta_x} \arccos\{\frac{1}{2} \exp[g(1 \mp \frac{3}{4}\lambda W + \frac{3}{16}\lambda^2 W^2)^{1/2} - g]\}$. The upper (lower) sector of the unit cell is topological (trivial), giving rise to an end mode and a domain wall mode at the charge neutrality point [Fig. 3(b)]. The end modes at all allowed momenta constitute a dispersionless band representing the edge state located at the stretched zigzag edge, while the domain wall modes result in a flat bulk band, which must be interpreted as the zeroth pseudo-Landau level, since no other bulk states are expected to be dispersionless. For the momenta $|k_x| > \hbar_{\max}^+$ ($|k_x| < \hbar_{\max}^-$), the unit cell realizes a purely topological (trivial) Su-Schrieffer-Heeger model [Fig. 3(b)]. When λ is increased to λ_c , the pseudo-Landau levels from the two valleys merge at the Brillouin zone center. The topological end modes on the stretched edge consequently constitute a flat band traversing the whole Brillouin zone [Fig. 3(c)]. Such a flat band persists [Fig. 3(d)] when λ is further increased to $\lambda_{\max} = 0.696W^{-1}$ corresponding

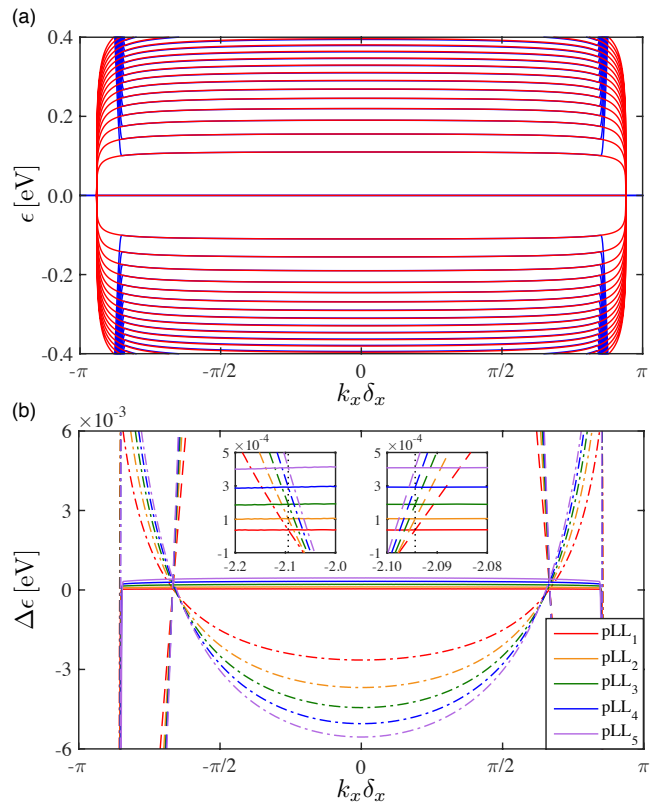


FIG. 4. (a) Band structure (blue) of a bent graphene nanoribbon of width $W = 511$ nm and maximal bend curvature $\lambda_{\max} = 1.36 \mu\text{m}^{-1}$. The red curves are the pseudo-Landau levels predicted by Eq. (7). (b) The energy differences between various analytically proposed pseudo-Landau levels $[\epsilon_n(k_x), \mathcal{E}_n^\eta(q_x), \text{ and } E_n^\eta]$ and the numerical energy bands in panel (a) are plotted as solid, dashed, and dot dashed curves, respectively. Left (right) inset enlarges the energy differences associated with $\epsilon_n(k_x)$ and E_n^η $[\mathcal{E}_n^\eta(q_x)]$ in the vicinity of the K point (dotted).

to the maximal bond elongation $\sim 27\%$ [31, 32].

Pseudo-Landau levels under strong strain.— In the presence of strong strain, the pseudo-Landau levels spread extensively in the Brillouin zone. The continuum Dirac theories [Eqs. (3) and (4)] obtained by linearizing the lattice Hamiltonian in the vicinity of the Brillouin zone corners consequently fail; and neither the Fermi velocity nor the pseudomagnetic field can be well defined. However, since the pseudo-Landau levels are well localized states, their dispersions can be in principle resolved by studying the physics in the vicinity of their guiding centers, which are the domain wall [Eq. (5)] in our case. Around the domain wall, the strain-modulated Hamiltonian [Eqs. (1) and (2)] is restored to a standard Dirac Hamiltonian

$$\hbar_{k_x, y} = \Omega(y - l_0)\sigma^x - it\delta_y\partial_y\sigma^y, \quad (6)$$

where $\Omega = [\frac{3}{4}\lambda g t(1 + \lambda l_0)]/\sqrt{\frac{3}{4}(1 + \lambda l_0)^2 + \frac{1}{4}}$. The resulting dispersive pseudo-Landau levels are (Sec. SIV of

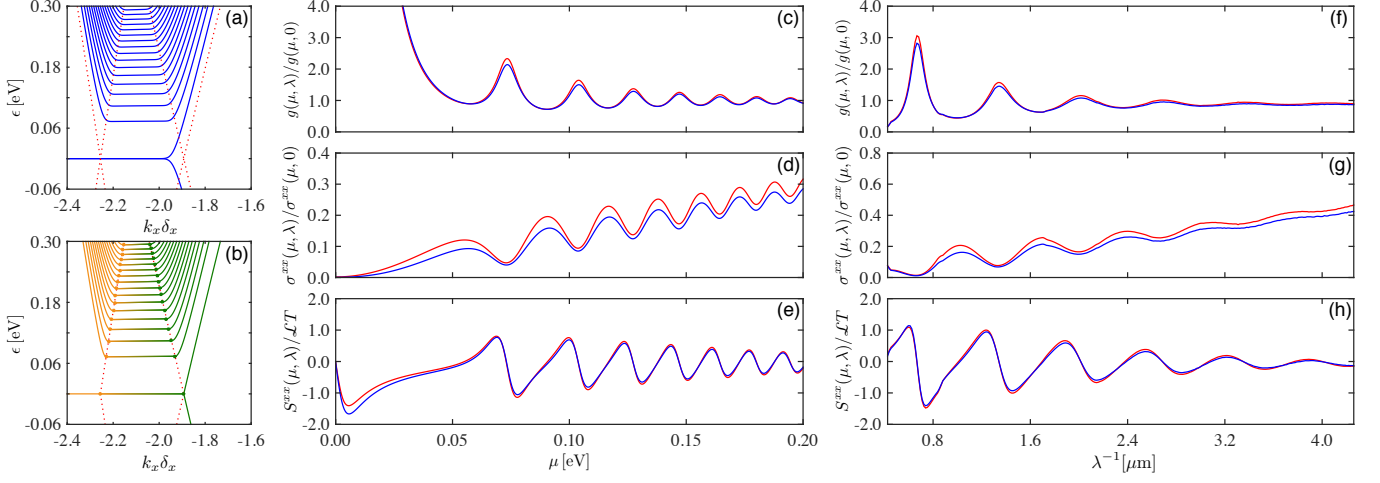


FIG. 5. Strain-induced quantum oscillations in a bent graphene nanoribbon of width $W = 192$ nm. (a) Numerically calculated bands (solid) at $\lambda = 0.642 \mu\text{m}^{-1}$ in the vicinity of the K point with maximally displaced Dirac cones (dotted). (b) Analytic band structure artificially constructed from Eqs. (7) and (8) resembles the numerical band structure in panel (a). Quantum oscillations of (c) DOS, (d) conductivity, (e) thermopower at fixed bend curvature $\lambda = 0.642 \mu\text{m}^{-1}$. Quantum oscillations of (f) DOS, (g) conductivity, (h) thermopower at fixed chemical potential $\mu = 0.112$ eV. In panels (c)-(h), the blue (red) curves represent the observables calculated from numerical (analytic) band structure in panel (a) [panel (b)] using Eq. (9); the parameter $\mathcal{L} = 2.45 \times 10^{-5}$ V/K²; and the data are broadened by convolving in energy a Lorentzian of width $\delta_\epsilon = 5.6$ meV to simulate the effects of disorder and finite temperature.

Ref. [42])

$$\epsilon_n(k_x) = \pm \sqrt{2n|\Omega t \delta_y|} = \pm \frac{3t}{2} \sqrt{ng\lambda a \sqrt{\frac{4}{3} - \frac{1}{3f_{k_x}^2}}}, \quad (7)$$

where $f_{k_x} = 1 + \frac{1}{g} \ln[2 \cos(\frac{1}{2}k_x \delta_x)]$. Equation (7) is our key result characterizing the dispersions of the pseudo-Landau levels at large (as well as small) λ . Its validity is justified by its good match to the numerically calculated energy bands in a wide range of momenta for a maximally bent graphene nanoribbon [Fig. 4(a)]. While Eq. (7) is derived from a nearest-neighbor model, we generalize it in Sec. SVI of Ref. [42] to incorporate various realistic effects such as the Semenoff mass [44–47], the spin-orbit coupling [48–50], the electric fields [51–58], and the next-nearest-neighbor hoppings [59].

We are surprised to find that the pseudo-Landau levels characterized by Eq. (7) deviate from the slightly dispersive ones $\mathcal{E}_n^\eta(q_x)$ even in the vicinity of the Brillouin zone corners [Fig. 4(b)], where they are expected to exhibit similar accuracy in fitting the numerics. More surprisingly, the deviation persists even in the weak strain limit (Sec. SV of Ref. [42]). This is because the linearization $t(y) \approx (1 - \frac{3}{4}\lambda gy)$ overlooks in Eq. (2) the higher-order terms [e.g., $O(\lambda^2 y^2)$], which can alter the pseudomagnetic field without impacting the Fermi velocity to the linear order of q_x (Sec. SV of Ref. [42]). This finding suggests that the widely used strain-modulated hoppings with linear space-dependence [13–15, 21, 28, 33, 37, 38] are inadequate in characterizing the pseudo-Landau level dispersions.

Pseudo-Landau-level-mediated transport.— To investigate the transport of the bent graphene nanoribbon, we also aspire to quantitatively understand the marginal energy bands spliced to the pseudo-Landau levels. Through the perturbation theory, we here treat such bands as pseudo-Landau-level-gapped chiral fermions with mass $\epsilon_n(k_n^{l,r})$, where k_n^l (k_n^r) marks the left (right) end of the n -th pseudo-Landau level at the valley K . Explicitly, the approximated dispersions read (Sec. SVIII of Ref. [42])

$$\epsilon_n^l(k_x) = \sqrt{t^2 \left[1 - \frac{\cos(\frac{1}{2}k_x \delta_x)}{\cos(\frac{1}{2}k_n^l \delta_x)} \right]^2 + [\epsilon_n(k_n^l)]^2}, \quad (8a)$$

$$\epsilon_n^r(k_x) = \sqrt{t^2 \left[1 - \frac{\cos(\frac{1}{2}k_x \delta_x)}{\cos(\frac{1}{2}k_n^r \delta_x)} \right]^2 + [\epsilon_n(k_n^r)]^2}. \quad (8b)$$

We note that Eqs. (7) and (8) together with flat edge bands at the neutrality point constitute an artificial band structure [Fig. 5(b)] highly mimicking the numerical one [Fig. 5(a)]. It thus should phenomenologically capture the transport of the numerical energy bands as well.

To substantiate our claim, we evaluate the density of states (DOS), electrical conductivity, and thermopower through [60, 61]

$$g(\mu, \lambda) = \sum_n \int \frac{dk_x}{2\pi} \delta[\epsilon_n^a(k_x) - \mu], \quad (9a)$$

$$\sigma^{xx}(\mu, \lambda) = e^2 \sum_n \int \frac{dk_x}{2\pi} (v_n^a)^2 \tau_n^a \delta[\epsilon_n^a(k_x) - \mu], \quad (9b)$$

$$S^{xx}(\mu, \lambda) = -\frac{\pi^2 k_B^2 T}{3e} \frac{d}{d\mu} \ln \sigma^{xx}(\mu, \lambda), \quad (9c)$$

where $\epsilon_n^a(k_x)$ denotes the artificial bands [Fig. 5(b)] composed of Eqs. (7) and (8); and $\tau_n^a = \tau_n[\epsilon_n^a(k_x), \lambda]$ is the relaxation time in the Boltzmann formalism [Eq. (9b)] and may be estimated as $\tau_n^a \approx C/g(\mu)$ with the parameter C determined by the scattering potential (Sec. SIX of Ref. [42]).

For a fixed bend curvature $\lambda = 0.642 \mu\text{m}^{-1}$, the analytically calculated DOS, conductivity, and thermopower from Eq. (9) are consistent with their counterparts numerically evaluated from the tight-binding Hamiltonian [Eq. (1)] with $t(y)$ substituting for $t_{1,2}$ [Figs. 5(c)-5(e)], justifying the validity of our approximated dispersions [Eq. (8)]. All the three quantities exhibit a series of peaks and dips when the chemical potential μ cuts through the dispersive pseudo-Landau levels. At a fixed chemical potential $\mu = 0.112 \text{eV}$, a scanned bend curvature pushes the pseudo-Landau levels through μ , resulting in a periodic electron population featured by the oscillating DOS [Fig. 5(f)]. The conductivity thus exhibits an unusual Shubnikov-de Haas oscillation in the complete absence of magnetic fields [Fig. 5(g)]. The oscillatory behavior is further passed to the Seebeck coefficient [Fig. 5(h)] through the Mott relation [Eq. (9c)].

It is worth noting that for certain values of λ that make the n -th pseudo-Landau level partially occupied, the conductivity $\sigma^{xx}(\mu, \lambda)$ decreases with an increasing $1/\lambda$, implying a *negative* strain-resistivity analogous to the negative magnetoresistivity in the chiral magnetic effect of Weyl semimetals [4–11]. This negative strain-resistivity is closely related to the dispersive pseudo-Landau levels [Eq. (7)], which play the same role as the chiral zeroth Landau levels in Weyl semimetals. Indeed, the partially filled n -th pseudo-Landau level contributes a bulk conductivity $\sigma_b^{xx}(\mu, \lambda) \sim (\frac{d\epsilon_n}{dk_x})^2 \mu$, which is an increasing function of λ (Sec. SIX of Ref. [42]). The pseudo-Landau-level-mediated intervalley transport reflects the non-conservation of the valley charge η , i.e., the valley anomaly [38], which is a direct manifestation of the $(1+1)$ -dimensional chiral anomaly [62].

Conclusions.— We analytically resolve the pseudo-Landau level dispersions in a strongly bent graphene nanoribbon and investigate their transport exemplified by the zero-field quantum oscillations and the negative strain-resistivity arising from the valley anomaly. Our findings may pave the way to graphene straintronics devices in the strong strain paradigm, which remains largely unexplored. Our techniques are transplantable to twisted two-dimensional materials and topological materials, especially the twisted bilayer graphene [63], Dirac superconductors [64–68], and bosonic “semimetals” [69–74], where pseudo-Landau levels have been reported.

The authors are indebted to H. Scherrer-Paulus, M. Franz, P. A. McClarty, X. -X. Zhang, É. Lantagne-Hurtubise, T. Matsushita, S. Fujimoto, Y. Chen, and Z. Shi for insightful discussions. T.L. gratefully acknowledges the scholarship from Max-Planck-Gesellschaft. H.-

Z.L. is supported by the National Natural Science Foundation of China (Grants No. 11534001, No. 11974249, and No. 11925402), the National Basic Research Program of China (Grant No. 2015CB921102), Guangdong Province (Grants No. 2016ZT06D348 and No. 2020KCX TD001), the National Key R & D Program (Grant No. 2016YFA0301700), Shenzhen High-Level Special Fund (Grants No. G02206304 and No. G02206404), and the Science, Technology and Innovation Commission of Shenzhen Municipality (Grants No. ZDSYS20170303165926217, No. JCYJ20170412152620376, and No. KYTDP20181011104202253).

-
- [1] L. D. Landau, “Diamagnetism of metals”, *Z. Physik* **64**, 629 (1930).
 - [2] K. v. Klitzing, G. Dorda, and M. Pepper, “New Method for High-Accuracy Determination of the Fine-Structure Constant Based on Quantized Hall Resistance”, *Phys. Rev. Lett.* **45**, 494 (1980).
 - [3] D. Shoenberg, *Magnetic Oscillations in Metals* (Cambridge University Press, Cambridge, 1984).
 - [4] K. Fukushima, D. E. Kharzeev, and H. J. Warringa, “Chiral magnetic effect”, *Phys. Rev. D* **78**, 074033 (2008).
 - [5] Q. Li, D. E. Kharzeev, C. Zhang, Y. Huang, I. Pletikosić, A. V. Fedorov, R. D. Zhong, J. A. Schneeloch, G. D. Gu, and T. Valla, “Chiral magnetic effect in ZrTe_5 ”, *Nat. Phys.* **12**, 550 (2016).
 - [6] A. A. Burkov, “Chiral anomaly and transport in Weyl metals”, *J. Phys.: Condens. Matter* **27**, 113201 (2015).
 - [7] D. T. Son and B. Z. Spivak, “Chiral anomaly and classical negative magnetoresistance of Weyl metals”, *Phys. Rev. B* **88**, 104412 (2013).
 - [8] X. Huang, L. Zhao, Y. Long, P. Wang, D. Chen, Z. Yang, H. Liang, M. Xue, H. Weng, Z. Fang, *et al.*, “Observation of the Chiral-Anomaly-Induced Negative Magnetoresistance in 3D Weyl Semimetal TaAs ”, *Phys. Rev. X* **5**, 031023 (2015).
 - [9] H.-J. Kim, K.-S. Kim, J.-F. Wang, M. Sasaki, N. Satoh, A. Ohnishi, M. Kitaura, M. Yang, and L. Li, “Dirac versus Weyl Fermions in Topological Insulators: Adler-Bell-Jackiw Anomaly in Transport Phenomena”, *Phys. Rev. Lett.* **111**, 246603 (2013).
 - [10] J. Xiong, S. K. Kushwaha, T. Liang, J. W. Krizan, M. Hirschberger, W. Wang, R. J. Cava, and N. P. Ong, “Evidence for the chiral anomaly in the Dirac semimetal Na_3Bi ”, *Science* **350**, 413 (2015).
 - [11] C.-L. Zhang, S.-Y. Xu, I. Belopolski, Z. Yuan, Z. Lin, B. Tong, G. Bian, N. Alidoust, C.-C. Lee, S.-M. Huang, *et al.*, “Signatures of the Adler-Bell-Jackiw chiral anomaly in a Weyl fermion semimetal”, *Nat. Commun.* **7**, 10735 (2016).
 - [12] M. A. H. Vozmediano, M. I. Katsnelson, and F. Guinea, “Gauge fields in graphene”, *Phys. Rep.* **496**, 109 (2010).
 - [13] R. Ilan, A. G. Grushin, and D. I. Pikulin, “Pseudo-electromagnetic fields in 3D topological semimetals”, *Nat. Rev. Phys.* **2**, 29 (2020).
 - [14] V. Arjona, E. V. Castro, and M. A. H. Vozmediano, “Collapse of Landau levels in Weyl semimetals”, *Phys.*

- Rev. B* **96**, 081110(R) (2017).
- [15] E. V. Castro, M. A. Cazalilla, and M. A. H. Vozmediano, “Raise and collapse of pseudo Landau levels in graphene”, *Phys. Rev. B* **96**, 241405(R) (2017).
- [16] B. Roy, Z.-X. Hu, and K. Yang, “Theory of unconventional quantum Hall effect in strained graphene”, *Phys. Rev. B* **87**, 121408(R) (2013).
- [17] B. Roy, F. F. Assaad, and I. F. Herbut, “Zero Modes and Global Antiferromagnetism in Strained Graphene”, *Phys. Rev. X* **4**, 021042 (2014).
- [18] B. Roy and J. D. Sau, “Competing charge-density wave, magnetic, and topological ground states at and near Dirac points in graphene in axial magnetic fields”, *Phys. Rev. B* **90**, 075427 (2014).
- [19] M. Oliva-Leyva, J. E. Barrios-Vargas, and G. G. de la Cruz, “Effective magnetic field induced by inhomogeneous Fermi velocity in strained honeycomb structures”, *Phys. Rev. B* **102**, 035447 (2020).
- [20] J. W. F. Venderbos and L. Fu, “Interacting Dirac fermions under a spatially alternating pseudomagnetic field: Realization of spontaneous quantum Hall effect”, *Phys. Rev. B* **93**, 195126 (2016).
- [21] M. Settnes, S. R. Power, and A.-P. Jauho, “Pseudomagnetic fields and triaxial strain in graphene”, *Phys. Rev. B* **93**, 035456 (2016).
- [22] F. Guinea, M. I. Katsnelson, and A. K. Geim, “Energy gaps and a zero-field quantum Hall effect in graphene by strain engineering”, *Nat. Phys.* **6**, 30 (2010).
- [23] N. Levy, S. A. Burke, K. L. Meaker, M. Panlasigui, A. Zettl, F. Guinea, A. H. C. Neto, and M. F. Crommie, “Strain-induced pseudo-magnetic fields greater than 300 Tesla in graphene nanobubbles”, *Science* **329**, 544 (2010).
- [24] J. Lu, A. H. C. Neto, and K. P. Loh, “Transforming Moiré blisters into geometric graphene nano-bubbles”, *Nat. Commun.* **3**, 823 (2012).
- [25] S.-Y. Li, K.-K. Bai, L.-J. Yin, J.-B. Qiao, W.-X. Wang, and L. He, “Observation of unconventional splitting of Landau levels in strained graphene”, *Phys. Rev. B* **92**, 245302 (2015).
- [26] N.-C. Yeh, M.-L. Teague, S. Yeom, B. Standley, R. T.-P. Wu, D. A. Boyd, and M. W. Bockrath, “Strain-induced pseudo-magnetic fields and charging effects on CVD-grown graphene”, *Surf. Sci.* **605**, 1649 (2011).
- [27] T. Liu, D. I. Pikulin, and M. Franz, “Quantum oscillations without magnetic field”, *Phys. Rev. B* **95**, 041201(R) (2017).
- [28] T. Liu, “Strain-induced pseudomagnetic field and quantum oscillations in kagome crystals”, *Phys. Rev. B* **102**, 045151 (2020).
- [29] D. I. Pikulin, A. Chen, and M. Franz, “Chiral Anomaly from Strain-Induced Gauge Fields in Dirac and Weyl Semimetals”, *Phys. Rev. X* **6**, 041021 (2016).
- [30] A. G. Grushin, J. W. F. Venderbos, A. Vishwanath, and R. Ilan, “Inhomogeneous Weyl and Dirac Semimetals: Transport in Axial Magnetic Fields and Fermi Arc Surface States from Pseudo-Landau Levels”, *Phys. Rev. X* **6**, 041046 (2016).
- [31] D.-B. Zhang, G. Seifert, and K. Chang, “Strain-Induced Pseudomagnetic Fields in Twisted Graphene Nanoribbons”, *Phys. Rev. Lett.* **112**, 096805 (2014).
- [32] J. H. Warner, E. R. Margine, M. Mukai, A. W. Robertson, F. Giustino, and A. I. Kirkland, “Dislocation-driven deformations in graphene”, *Science* **337**, 209 (2012).
- [33] F. Guinea, A. K. Geim, M. I. Katsnelson, and K. S. Novoselov, “Generating quantizing pseudomagnetic fields by bending graphene ribbons”, *Phys. Rev. B* **81**, 035408 (2010).
- [34] Y. Chang, T. Albash, and S. Haas, “Quantum Hall states in graphene from strain-induced nonuniform magnetic fields”, *Phys. Rev. B* **86**, 125402 (2012).
- [35] S. G. Stuij, P. H. Jacobse, V. Juričić, and C. M. Smith, “Tuning edge state localization in graphene nanoribbons by in-plane bending”, *Phys. Rev. B* **92**, 075424 (2015).
- [36] Z. Shi, H.-Z. Lu, and T. Liu, “Pseudo Landau levels, negative strain resistivity, and enhanced thermopower in twisted graphene nanoribbons”, *Phys. Rev. Research* **3**, 033139 (2021).
- [37] Y.-H. Ho, E. V. Castro, and M. A. Cazalilla, “Haldane model under nonuniform strain”, *Phys. Rev. B* **96**, 155446 (2017).
- [38] É. Lantagne-Hurtubise, X.-X. Zhang, and M. Franz, “Dispersive Landau levels and valley currents in strained graphene nanoribbons”, *Phys. Rev. B* **101**, 085423 (2020).
- [39] S. Ryu and Y. Hatsugai, “Topological Origin of Zero-Energy Edge States in Particle-Hole Symmetric Systems”, *Phys. Rev. Lett.* **89**, 077002 (2002).
- [40] W. P. Su, J. R. Schrieffer, and A. J. Heeger, “Solitons in Polyacetylene”, *Phys. Rev. Lett.* **42**, 1698 (1979).
- [41] A. H. Castro Neto, F. Guinea, N. M. R. Peres, K. S. Novoselov, and A. K. Geim, “The electronic properties of graphene”, *Rev. Mod. Phys.* **81**, 109 (2009).
- [42] See Supplemental Material for details.
- [43] V. M. Pereira, A. H. Castro Neto, and N. M. R. Peres, “Tight-binding approach to uniaxial strain in graphene”, *Phys. Rev. B* **80**, 045401 (2009).
- [44] G. W. Semenoﬀ, “Condensed-Matter Simulation of a Three-Dimensional Anomaly”, *Phys. Rev. Lett.* **53**, 2449 (1984).
- [45] G. Giovannetti, P. A. Khomyakov, G. Brocks, P. J. Kelly, and J. van den Brink, “Substrate-induced band gap in graphene on hexagonal boron nitride: *Ab initio* density functional calculations”, *Phys. Rev. B* **76**, 073103 (2007).
- [46] S. Y. Zhou, G.-H. Gweon, A. V. Fedorov, P. N. First, W. A. De Heer, D.-H. Lee, F. Guinea, A. H. Castro Neto, and A. Lanzara, “Substrate-induced bandgap opening in epitaxial graphene”, *Nat. Mater.* **6**, 770 (2007).
- [47] P. Nigge, A. Qu, É. Lantagne-Hurtubise, E. Mårsell, S. Link, G. Tom, M. Zonno, M. Michiardi, M. Schneider, S. Zhdanovich, *et al.*, “Room temperature strain-induced Landau levels in graphene on a wafer-scale platform”, *Sci. Adv.* **5**, eaaw5593 (2019).
- [48] C. L. Kane and E. J. Mele, “Quantum Spin Hall Effect in Graphene”, *Phys. Rev. Lett.* **95**, 226801 (2005).
- [49] H. Min, J. E. Hill, N. A. Sinitsyn, B. R. Sahu, L. Kleinman, and A. H. MacDonald, “Intrinsic and Rashba spin-orbit interactions in graphene sheets”, *Phys. Rev. B* **74**, 165310 (2006).
- [50] F. D. M. Haldane, “Model for a Quantum Hall Effect without Landau Levels: Condensed-Matter Realization of the “Parity Anomaly””, *Phys. Rev. Lett.* **61**, 2015 (1988).
- [51] N. M. R. Peres and E. V. Castro, “Algebraic solution of a graphene layer in transverse electric and perpendicular magnetic fields”, *J. Phys.: Condens. Matter* **19**, 406231 (2007).
- [52] V. Lukose, R. Shankar, and G. Baskaran, “Novel Electric

- Field Effects on Landau Levels in Graphene”, *Phys. Rev. Lett.* **98**, 116802 (2007).
- [53] Y. A. Bychkov and E. I. Rashba, “Oscillatory effects and the magnetic susceptibility of carriers in inversion layers”, *J. Phys. C: Solid State Phys.* **17**, 6039 (1984).
- [54] D. Huertas-Hernando, F. Guinea, and A. Brataas, “Spin-orbit coupling in curved graphene, fullerenes, nanotubes, and nanotube caps”, *Phys. Rev. B* **74**, 155426 (2006).
- [55] Y. S. Dedkov, M. Fonin, U. Rüdiger, and C. Laubschat, “Rashba Effect in the Graphene/Ni(111) System”, *Phys. Rev. Lett.* **100**, 107602 (2008).
- [56] S. Konschuh, M. Gmitra, and J. Fabian, “Tight-binding theory of the spin-orbit coupling in graphene”, *Phys. Rev. B* **82**, 245412 (2010).
- [57] M. Zarea and N. Sandler, “Rashba spin-orbit interaction in graphene and zigzag nanoribbons”, *Phys. Rev. B* **79**, 165442 (2009).
- [58] J. C. Boettger and S. B. Trickey, “First-principles calculation of the spin-orbit splitting in graphene”, *Phys. Rev. B* **75**, 121402(R) (2007).
- [59] S. Reich, J. Maultzsch, C. Thomsen, and P. Ordejón, “Tight-binding description of graphene”, *Phys. Rev. B* **66**, 035412 (2002).
- [60] N. W. Ashcroft and N. D. Mermin, *Solid State Physics* (Saunders College, Philadelphia, 1976).
- [61] M. Cutler and N. F. Mott, “Observation of Anderson Localization in an Electron Gas”, *Phys. Rev.* **181**, 1336 (1969).
- [62] H. B. Nielsen and M. Ninomiya, “The Adler-Bell-Jackiw anomaly and Weyl fermions in a crystal”, *Phys. Lett. B* **130**, 389 (1983).
- [63] J. Liu, J. Liu, and X. Dai, “Pseudo Landau level representation of twisted bilayer graphene: Band topology and implications on the correlated insulating phase”, *Phys. Rev. B* **99**, 155415 (2019).
- [64] T. Liu, M. Franz, and S. Fujimoto, “Quantum oscillations and Dirac-Landau levels in Weyl superconductors”, *Phys. Rev. B* **96**, 224518 (2017).
- [65] T. Kobayashi, T. Matsushita, T. Mizushima, A. Tsuruta, and S. Fujimoto, “Negative Thermal Magnetoresistivity as a Signature of a Chiral Anomaly in Weyl Superconductors”, *Phys. Rev. Lett.* **121**, 207002 (2018).
- [66] T. Matsushita, T. Liu, T. Mizushima, and S. Fujimoto, “Charge/spin supercurrent and the Fulde-Ferrell state induced by crystal deformation in Weyl/Dirac superconductors”, *Phys. Rev. B* **97**, 134519 (2018).
- [67] G. Massarelli, G. Wachtel, J. Y. T. Wei, and A. Paramakanti, “Pseudo-Landau levels of Bogoliubov quasiparticles in strained nodal superconductors”, *Phys. Rev. B* **96**, 224516 (2017).
- [68] E. M. Nica and M. Franz, “Landau levels from neutral Bogoliubov particles in two-dimensional nodal superconductors under strain and doping gradients”, *Phys. Rev. B* **97**, 024520 (2018).
- [69] T. Liu and Z. Shi, “Strain-induced dispersive Landau levels: Application in twisted honeycomb magnets”, *Phys. Rev. B* **103**, 144420 (2021).
- [70] T. Liu and Z. Shi, “Magnon quantum anomalies in Weyl ferromagnets”, *Phys. Rev. B* **99**, 214413 (2019).
- [71] Y. Ferreira and M. A. H. Vozmediano, “Elastic gauge fields and Hall viscosity of Dirac magnons”, *Phys. Rev. B* **97**, 054404 (2018).
- [72] M. C. Rechtsman, J. M. Zeuner, A. Tünnermann, S. Nolte, M. Segev, and A. Szameit, “Strain-induced pseudomagnetic field and photonic Landau levels in dielectric structures”, *Nat. Photon.* **7**, 153 (2013).
- [73] X. Wen, C. Qiu, Y. Qi, L. Ye, M. Ke, F. Zhang, and Z. Liu, “Acoustic Landau quantization and quantum-Hall-like edge states”, *Nat. Phys.* **15**, 352 (2019).
- [74] C. Brendel, V. Peano, O. J. Painter, and F. Marquardt, “Pseudomagnetic fields for sound at the nanoscale”, *Proc. Natl. Acad. of Sci. U.S.A.* **114**, E3390 (2017).